Topological phases in $ZrTe_5$ and chirality enabled quantum information systems

Qiang Li

Department of Physics and Astronomy, Stony Brook University

Condensed Matter Physics and Materials Science Division, Brookhaven National Laboratory

Acknowledgements:

Collaborators/Group Members at Brookhaven National Lab and Stony Brook University

Single crystals and thin films


Genda Gu


Shannon Lee

Optical and electron spectroscopy (ARPES)


Mengkun Liu


Peter Johnson (R)


Dan Nevola


Michael Dapolito


Jigang Wang (Ames Lab & Iowa State University)

Quantum transport

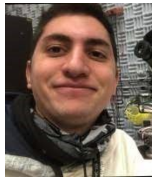
Pedro Lozano


Juntao Yao

Theory/computation


Weiguo Yi


Niraj Arya

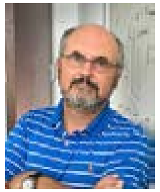
Alexei Tsvelik


Dmitri Kharzeev

This work was supported by the U.S. Department of Energy (DOE), Office of Basic Energy Sciences, Division of Materials Sciences and Engineering, under Contract No. DE-SC0012704.

Outline

- Chiral (Dirac/Weyl) semimetals and topological insulators
- Topological phase transitions
- Quantum computing with chiral fermions

Chirality:

(electrons, quarks, and neutrinos)

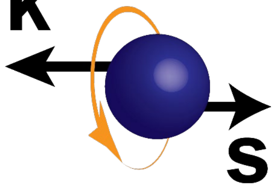

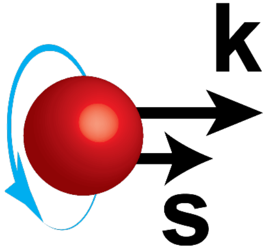

Left-handed **Right-handed**

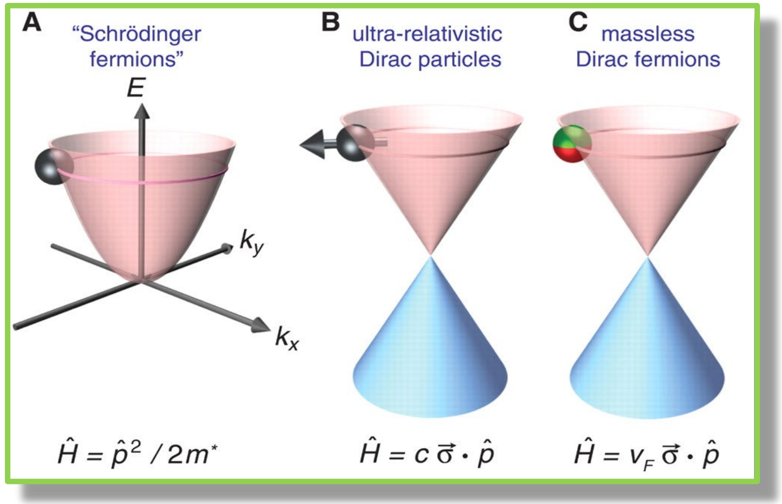

A. K. Geim, Science 324,1530 (2009)

3D semimetals with linear dispersion

Weyl semimetal
(non-degenerated bands)

Dirac semimetal
(doubly degenerated bands)

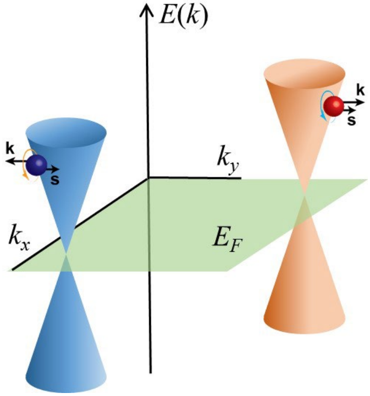

TaAs
NbAs
NbP
TaP

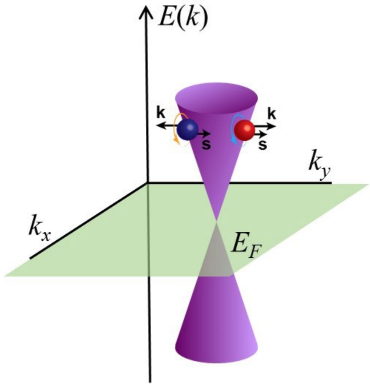

$ZrTe_5$
Na_3Bi,
Cd_3As_2

- The Dirac point can split into two Weyl points either by breaking the crystal inversion symmetry or time-reversal symmetry.
- Each Weyl point acts like a singularity of the Berry curvature in the Brillion Zone – magnetic monopole in *k*-space

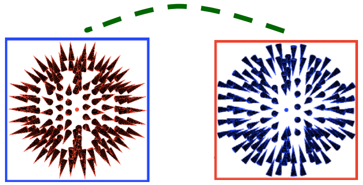

Chiral Magnetic Effect (CME) in Condensed Matters (CM)

Dmitri Kharzeev
(SBU/BNL)

The generation of electric current by the chirality imbalance between left- and right-handed fermions in an external magnetic field.

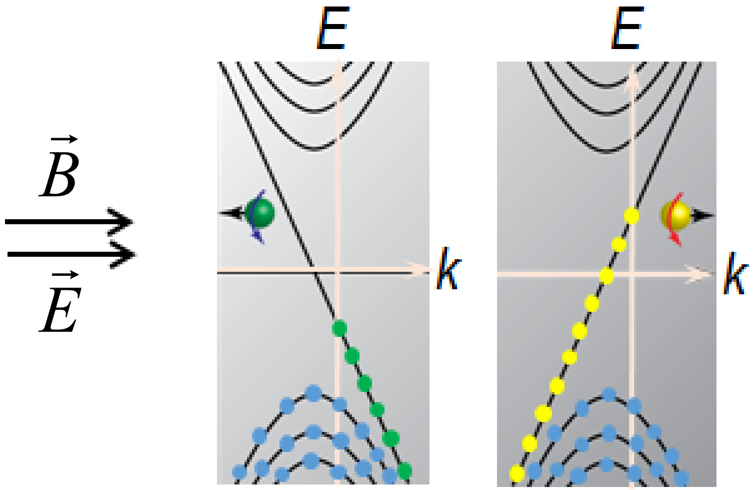

Chiral magnetic current: $\vec{J}_{CME} = \frac{e^2}{2\pi^2}\mu_5\vec{B}$

$$J^i_{CME} = \boxed{\frac{e^2}{\pi\hbar}\frac{3}{8}\frac{e^2}{\hbar c}\frac{v^3}{\pi^3}\frac{\tau_v}{T^2+\frac{\mu^2}{\pi^2}}B^iB^k}E^k = \boxed{\sigma^{ik}_{CME}}E^k$$

$$\sigma^{xx}_{CME} = \frac{e^2}{\pi\hbar}\frac{3}{8}\frac{e^2}{\hbar c}\frac{v^3}{\pi^3}\frac{\tau_v}{T^2+\frac{\mu^2}{\pi^2}}B^2 = \alpha(T)\cdot B^2$$

A negative longitudinal magnetoresistance (NLMR) at $(\vec{B}//\vec{E})$ in Dirac/Weyl semimetals

Chiral anomaly and chiral magnetic effect

$$\vec{J}_{CME} = \frac{e^2}{2\pi^2}\mu_5 \vec{B}$$

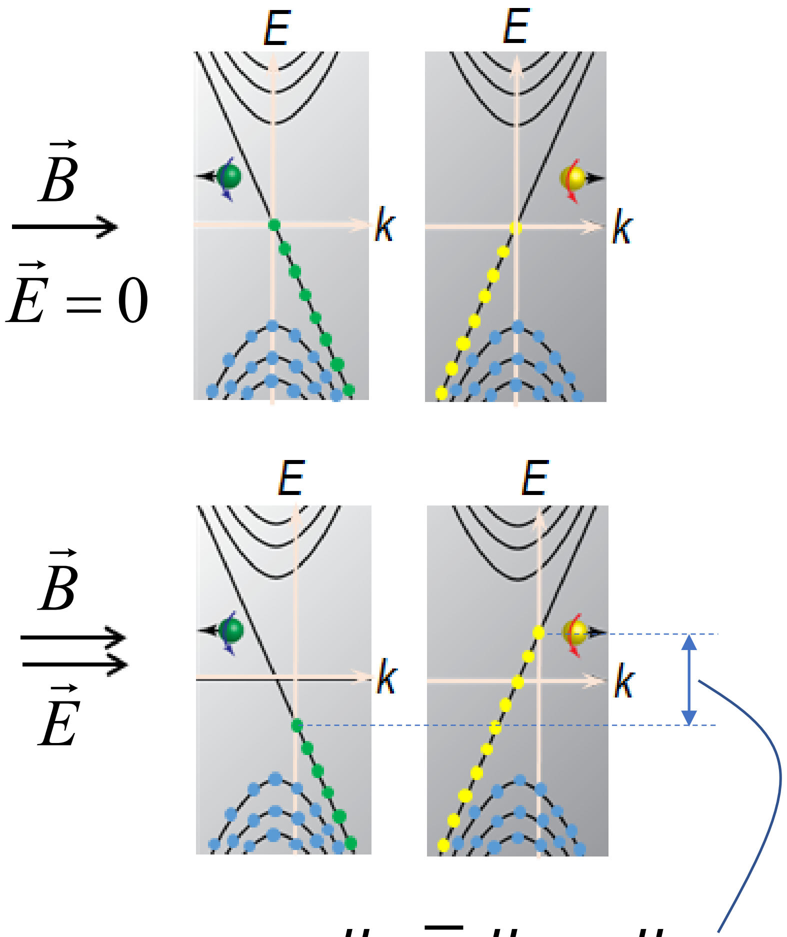

$$\mu_5 \equiv \mu_R - \mu_L$$

Adler-Bell-Jackiw anomaly

Adler, Phys. Rev. 177, 2426 (1969)
Bell & Jackiw, Nuov Cim 60, 47–61 (1969)

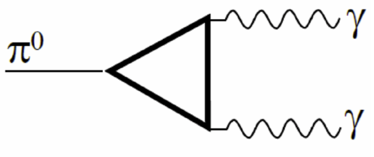

Rapid decay of π^o into two photons γ

Nielsen and Ninomiya (1983) - Physics Letters B130, 389 (1983)

"The Adler-Bell-Jackiw anomaly and **Weyl** fermions in a crystal"

Son and Spivak (2013) - Phys. Rev. B, 88, 104412 (2013).

"Chiral anomaly and classical negative magnetoresistance of Weyl metals."

Burkov (2014) -Phys. Rev. Lett., 113, 247203 (2014).

"Chiral anomaly and diffusive magneto-transport in Weyl metals".

Discovery of chiral magnetic effect in $ZrTe_5$

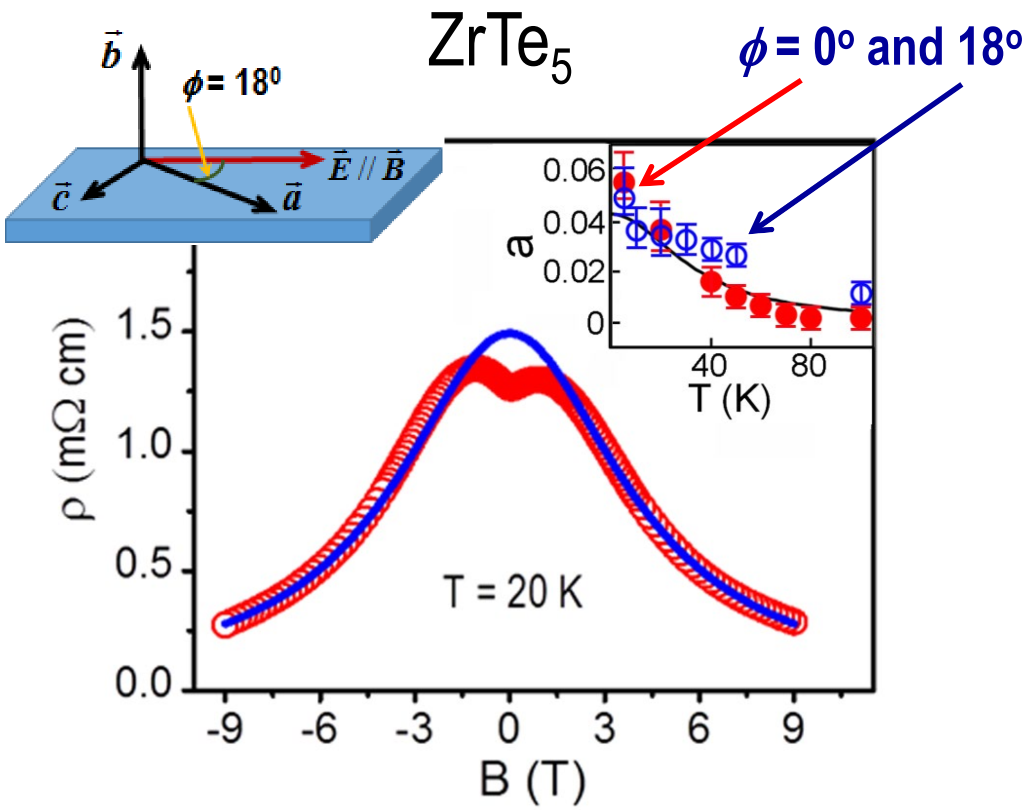

$$\sigma = \sigma_0 + \sigma_{CME}$$

$$\sigma_{CME}^{zz} = \frac{e^2}{\pi\hbar}\frac{3}{8}\frac{e^2}{\hbar c}\frac{v^3}{\pi^3}\frac{\tau_V}{T^2+\frac{\mu^2}{\pi^2}}B^2 = a(T)B^2$$

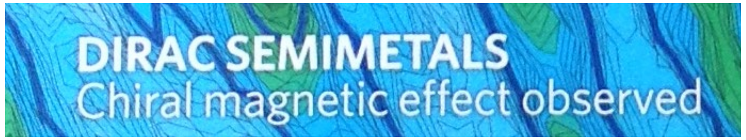

QL, Kharzeev, et al arXiv:1412.6543, Nature Physics 12 550 (2016)

Zirconium Pentatelluride $ZrTe_5$

Crystal structure

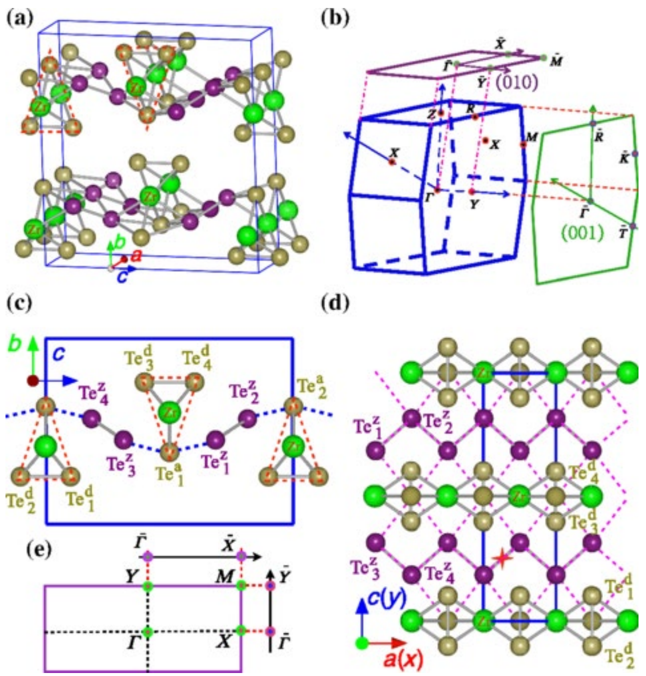

2D topological insulator
(monolayer – prediction)

Weng et al. Phys. Rev. **X** 4, 011002 (2014)

Electronic structure

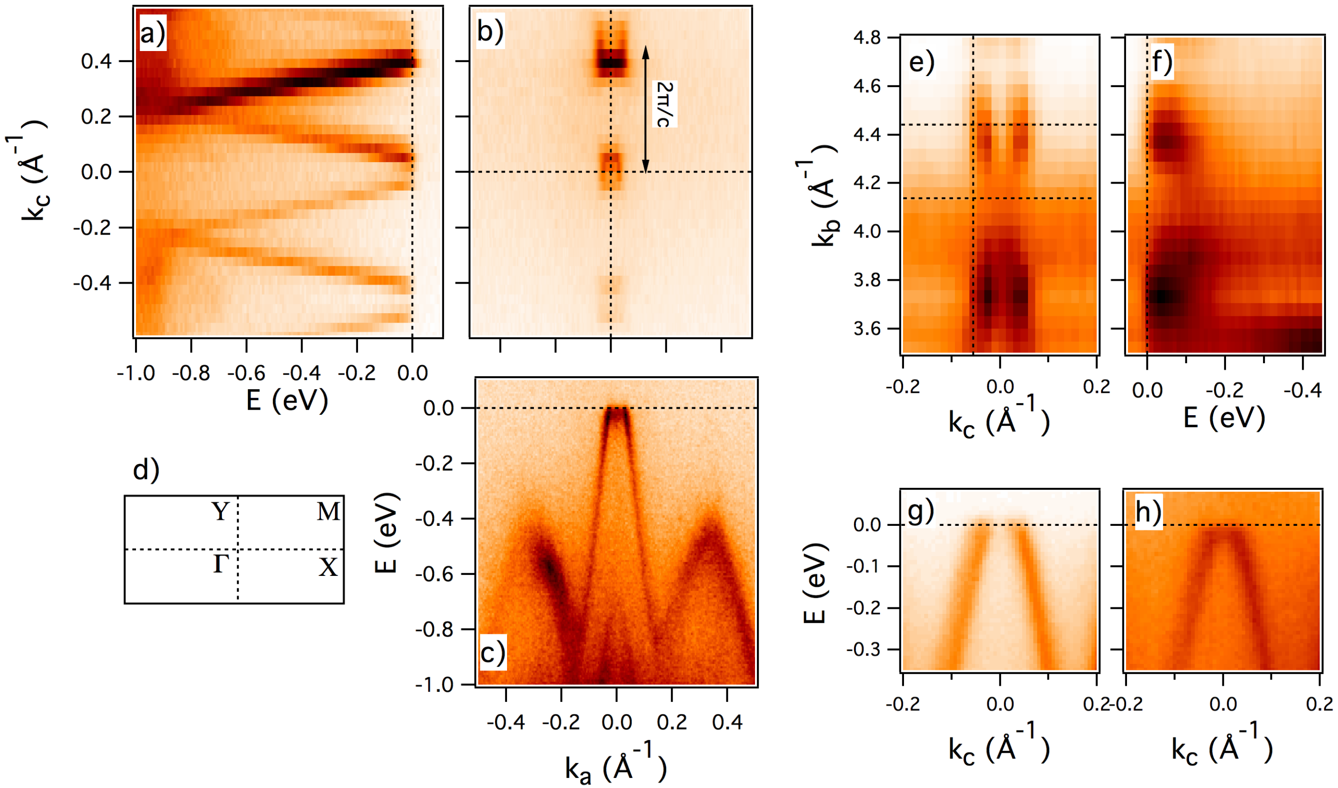

Dirac semimetal dispersion (ARPES)

Li et al. arXiv:1412.6543, Nature Physics 12 550 (2016)

Magneto-transport properties of $ZrTe_5$

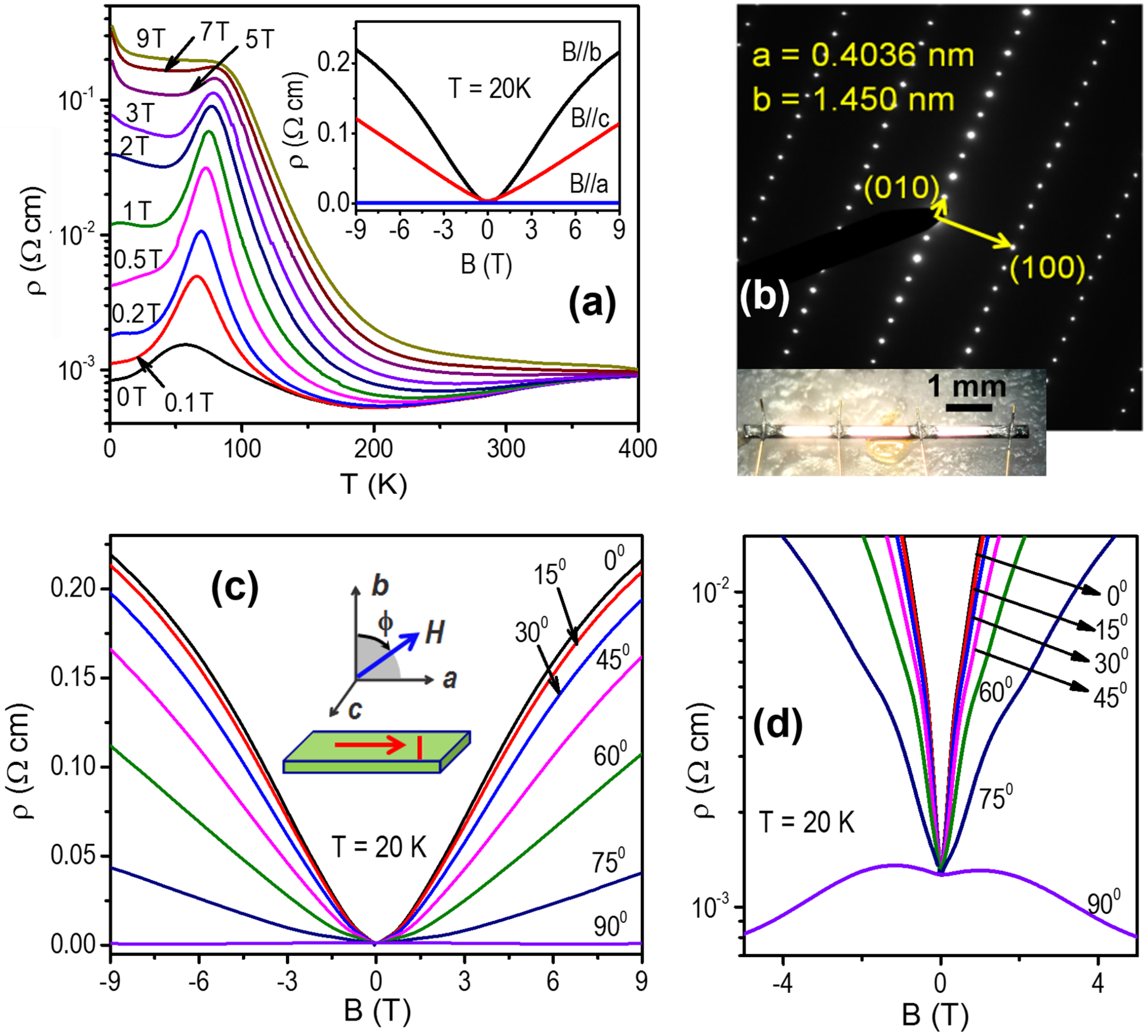

Measurable parameter from CME

Large negative magnetoresistance

when B//E ($\phi = 90^o$)

Li, et al arXiv:1412.6543, Nature Physics (2016) doi:10.1038/nphys3648

Magneto-terahertz spectroscopy (non contact) confirmed the chiral anomaly in a Dirac semimetal Cd_3As_2

"Intrinsic dc magnetoconductivity from chiral anomaly in sample S1 (blue) and sample S2 (red). In both samples, $\Delta\sigma$ follows B^2"

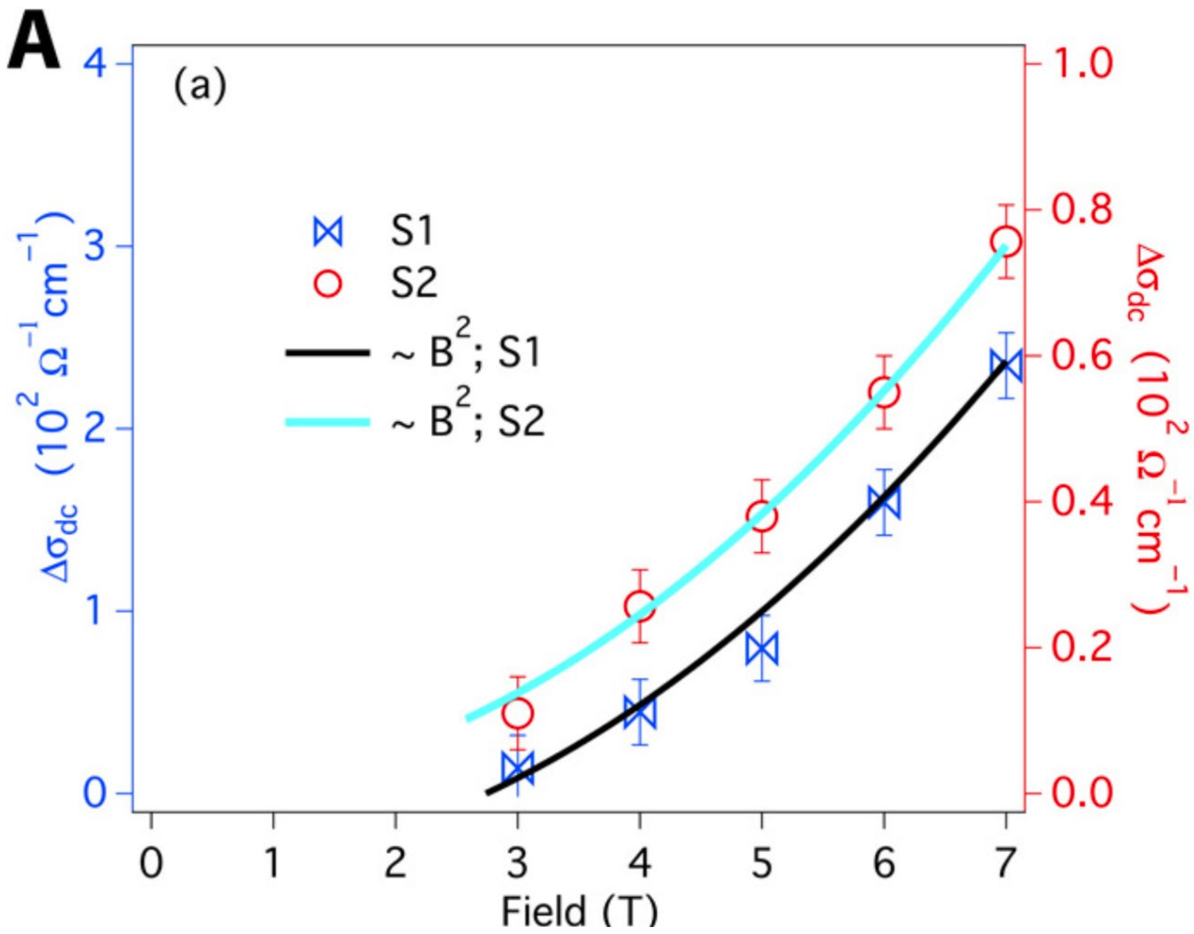

Cheng, Armitage et al., SCIENCE ADVANCES, 7 abg0914 (2021)

Topological states in $ZrTe_5$

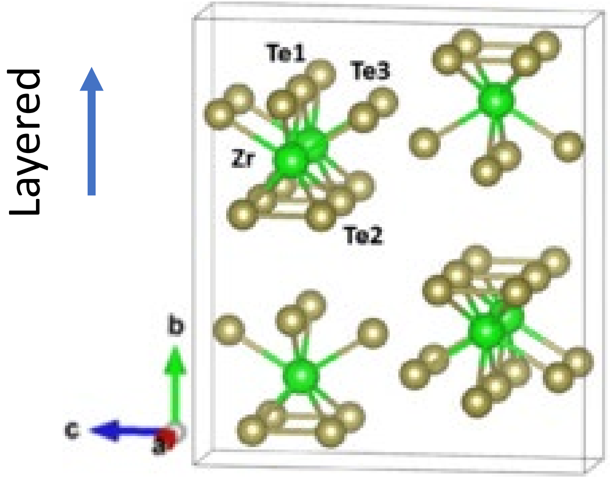

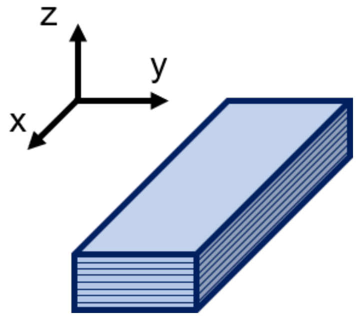

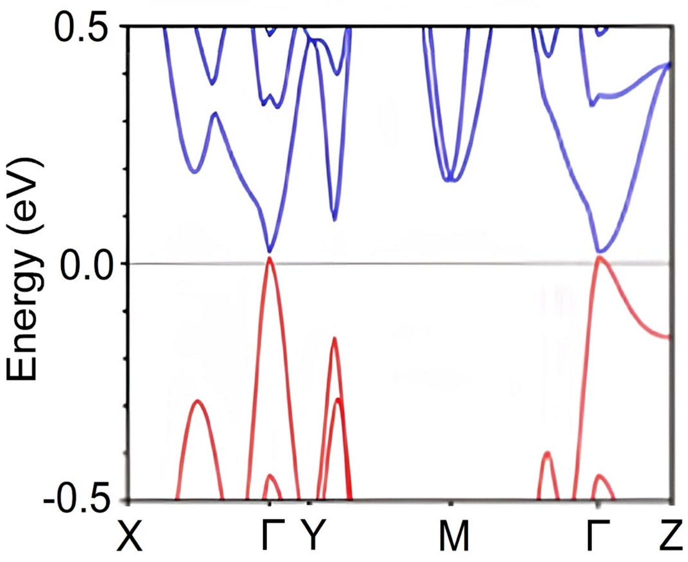

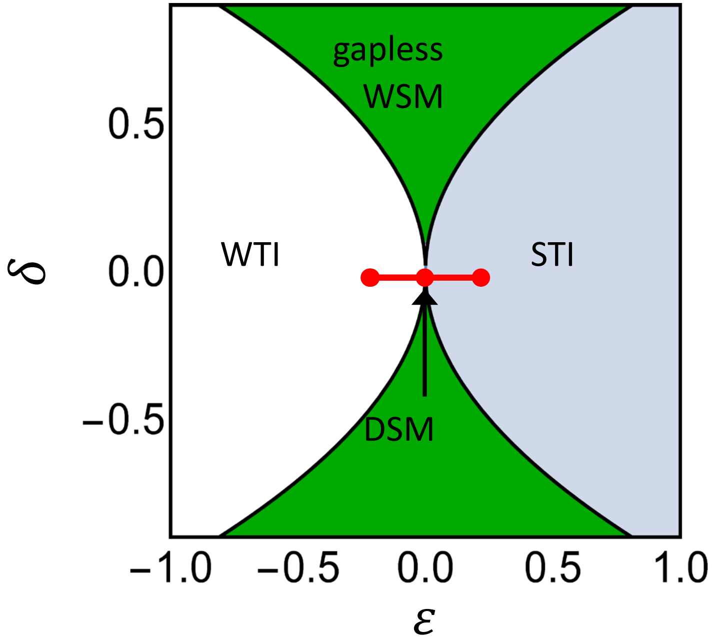

Ref. P. Zhang, QL et al., Nat. Commun. 12, 406 (2021)
N. Aryal, QL et al., Phys. Rev. Lett. 126, 016401 (2021)

Strain Induced Topological Phase Transition in $ZrTe_5$

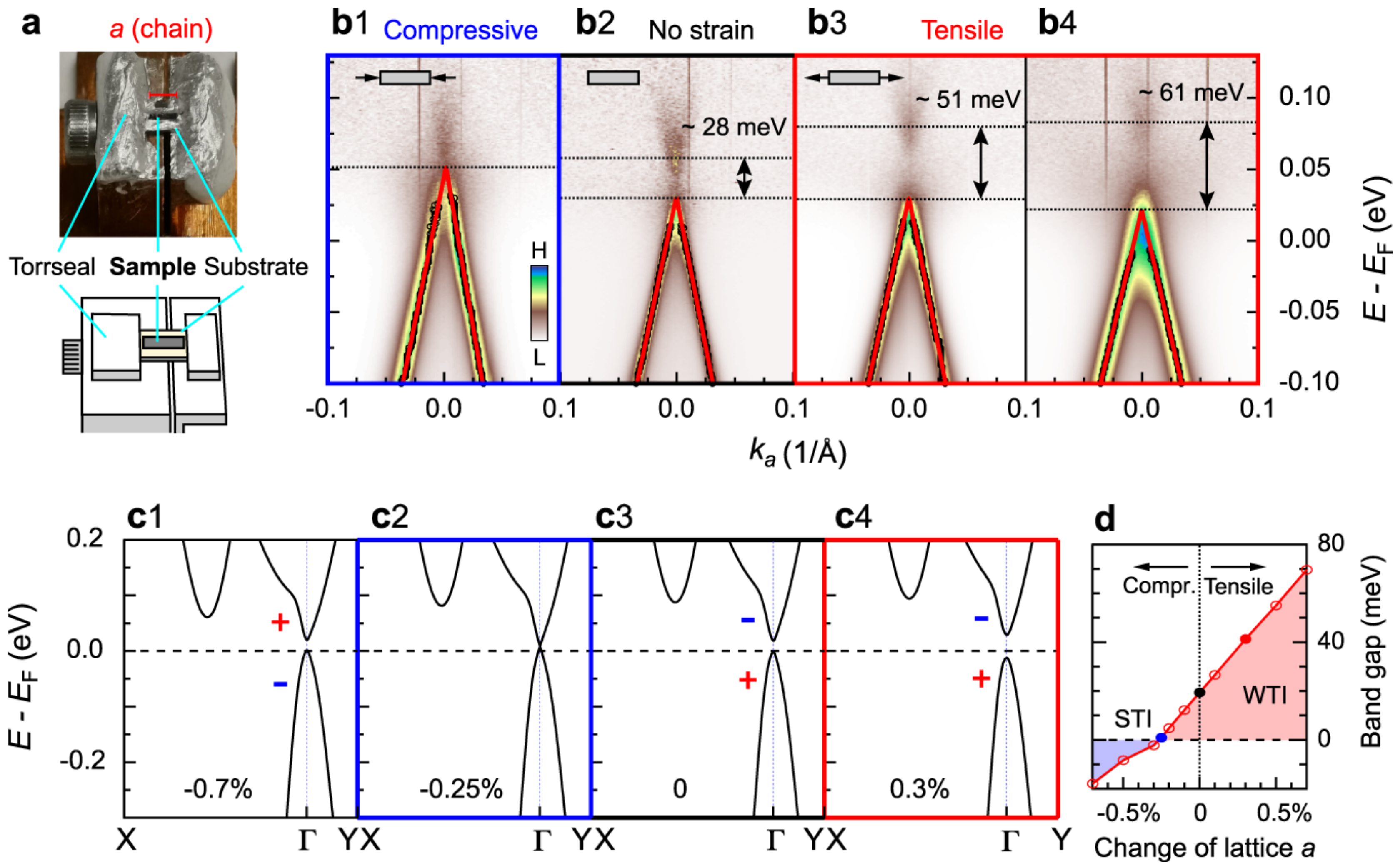

a) The strain device.

b) Bulk band gap change with compressive and tensile strain. The data are taken with p-polarized photons. The black markers are extracted from the MDC peaks, and the red solid lines are the fitting results

c) Calculated band structure with different lattice constant a. + and − signs indicate the parity of the two bands.

d) Calculated phase diagram with different lattice constant (strain). Blue, black, and red solid markers roughly indicate the experimental values in b.

Zhang, QL, et al. *Nature Communications* **12,** 406 (2021)

$ZrTe_5$ - Light dark matter detection

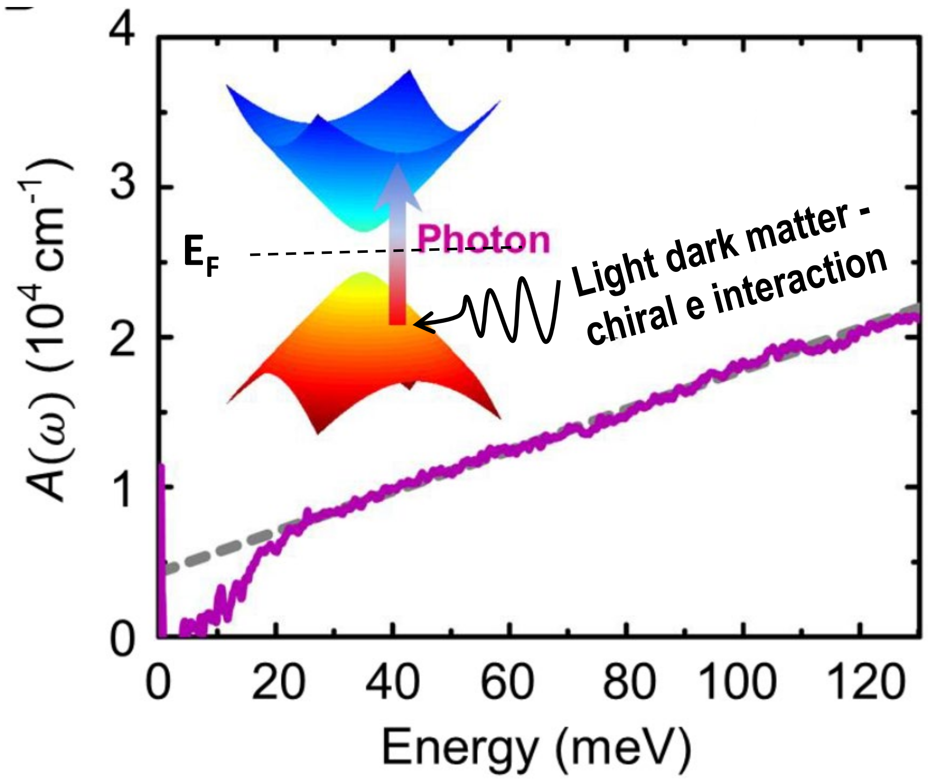

- At no thermal excitation
- Fermi level in the gap Δ

(12.4 meV ~ 3 THz)

$ZrTe_5$

Light dark matter detection

More on topological states in $ZrTe_5$

3D weak topological insulator

Zhang, QL, et al. Nature Communications 12, 406 (2021)

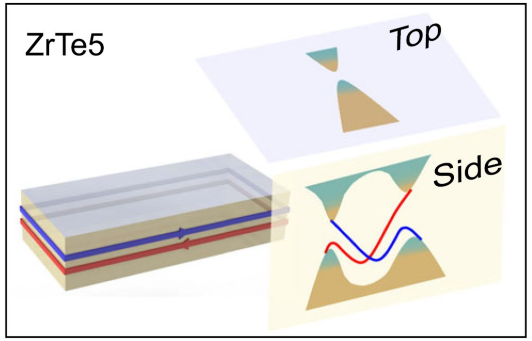

Dynamic Dirac/Weyl semimetal

Aryal, QL, et al. Phys. Rev. Lett. 126, 016401 (2021)

Vaswani, QL, et al. Phys. Rev. X 10, 021013 (2020)

Luo, QL, et al. Nature Materials 20, 329 (2021)

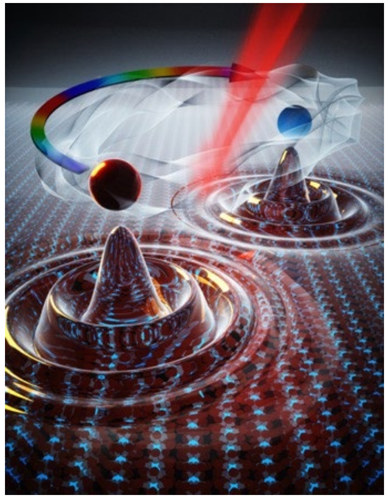

3D quantum Hall effect

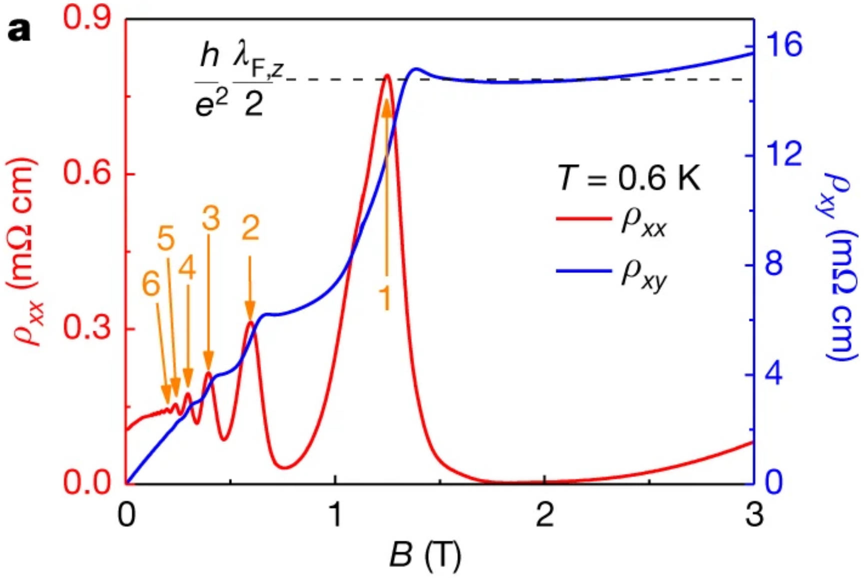

Tang et al. Nature 569, 537 (2019).

Galeski, QL et al. Nat. Commun.12, 1 (2021)

Coherent Phonon Control of Topological Phase Transition in $ZrTe_5$

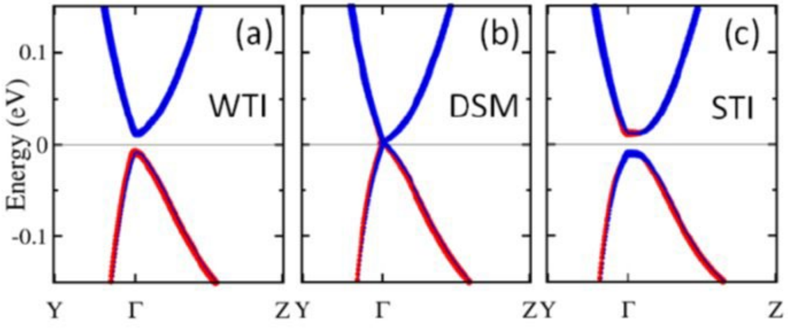

Evolution of the band structure around the Γ point for different values of the normal coordinate Q corresponding to the Ag-27 Raman-active phonon mode.

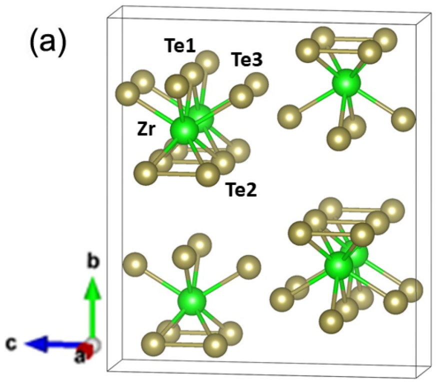

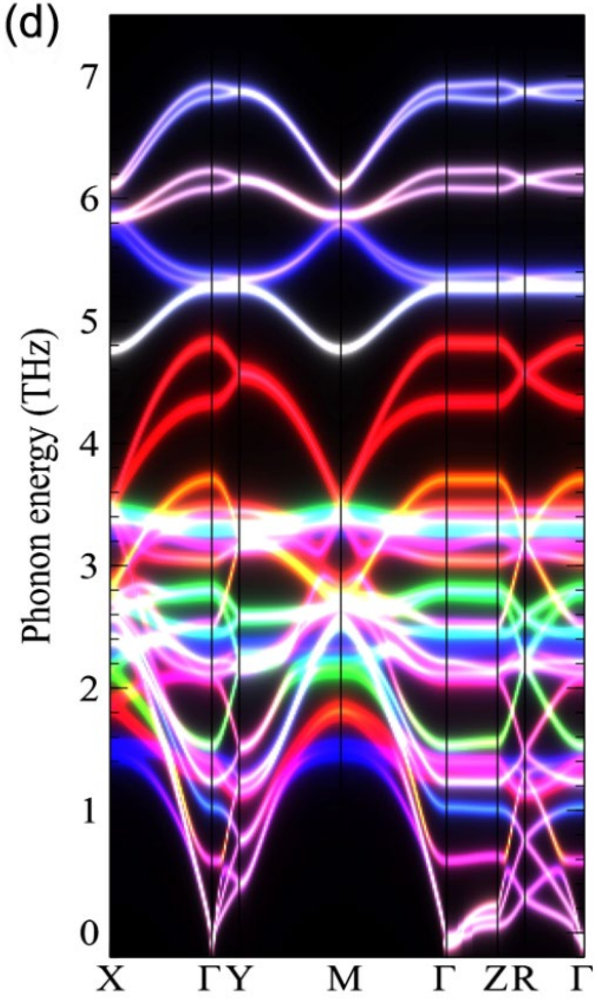

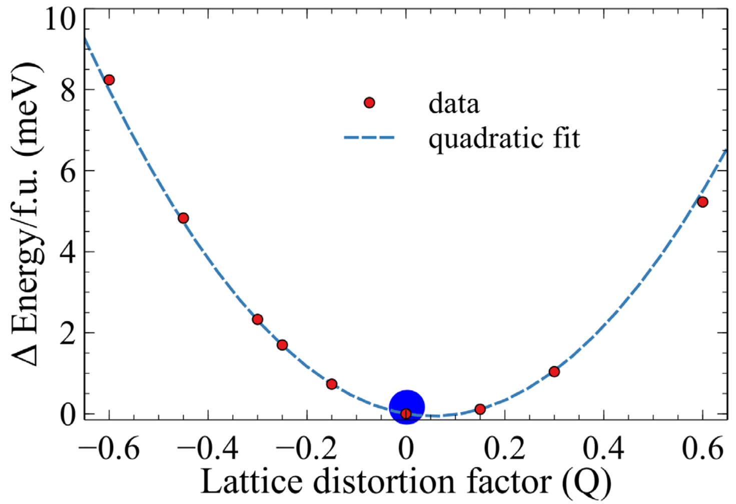

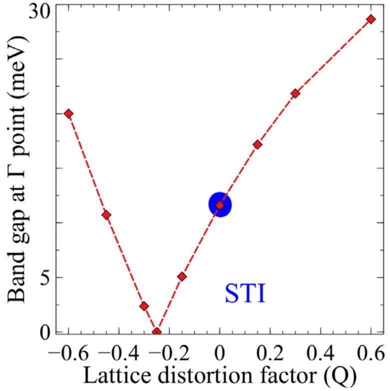

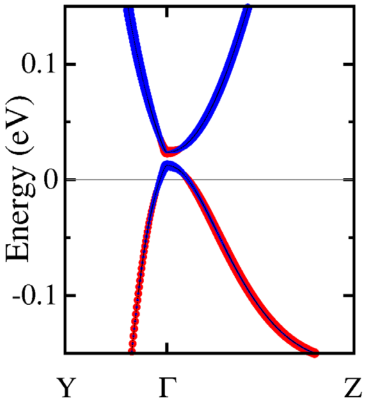

Aryal, Li, et al Phys. Rev. Lett. 126, 016401 (2021)

Light-Driven Ultrafast Topology Switching in $ZrTe_5$

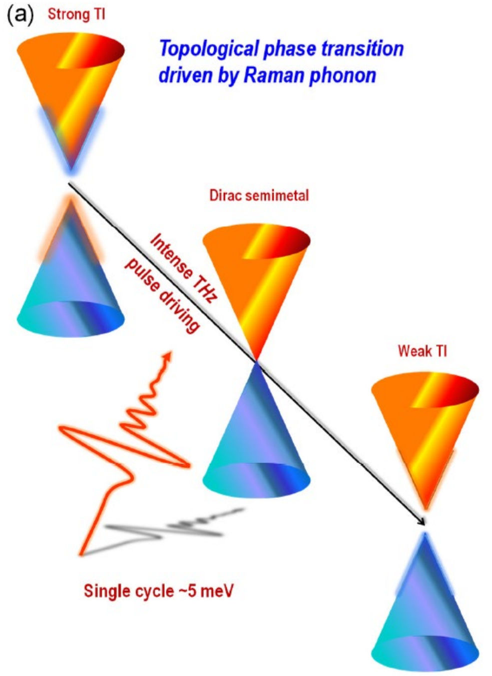

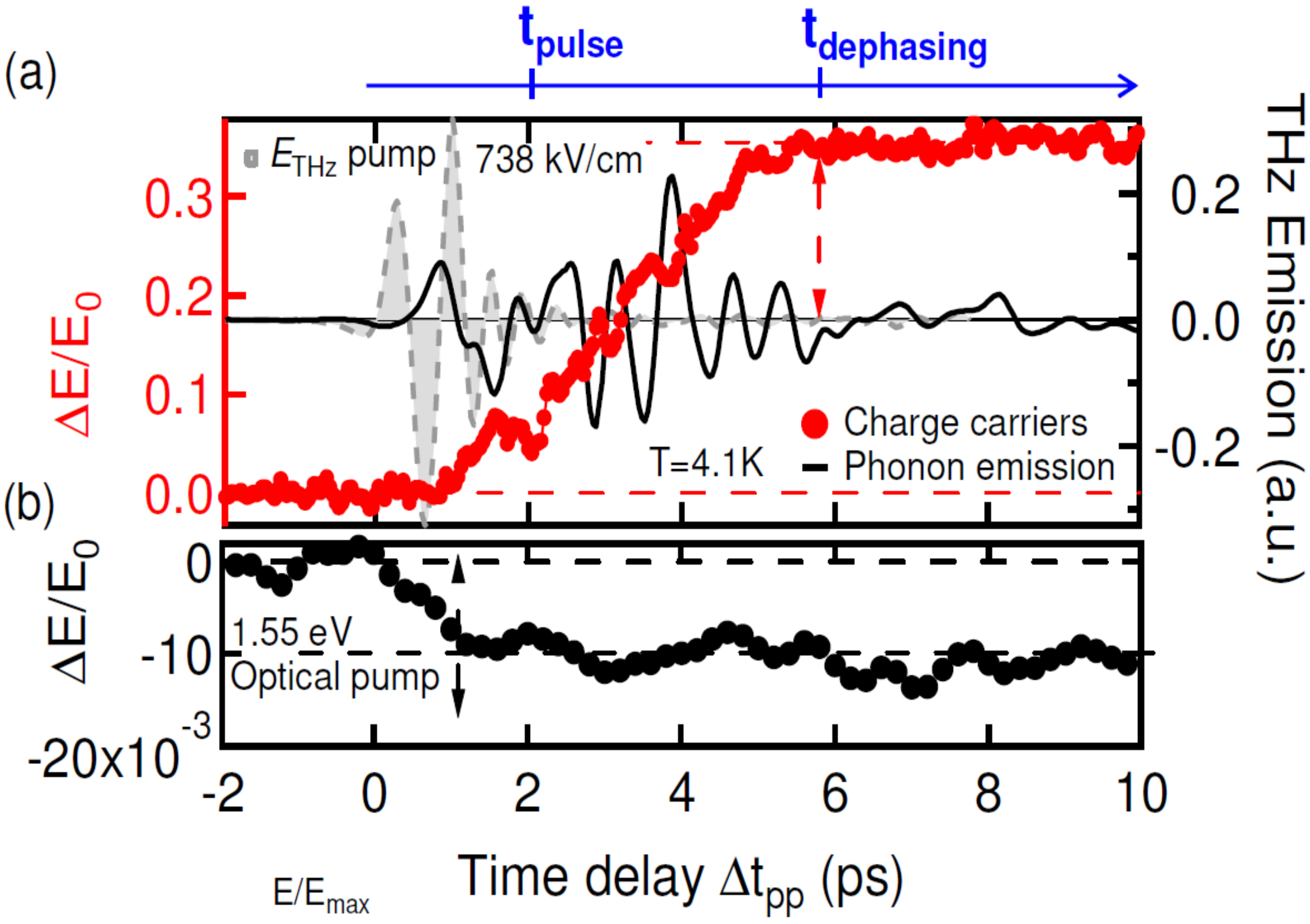

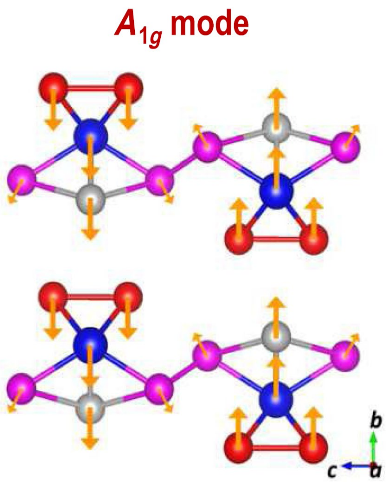

Vaswani, QL, et al. Physical Review X 10, 021013 (2020)

Phonon induced Weyl phases in $ZrTe_5$*

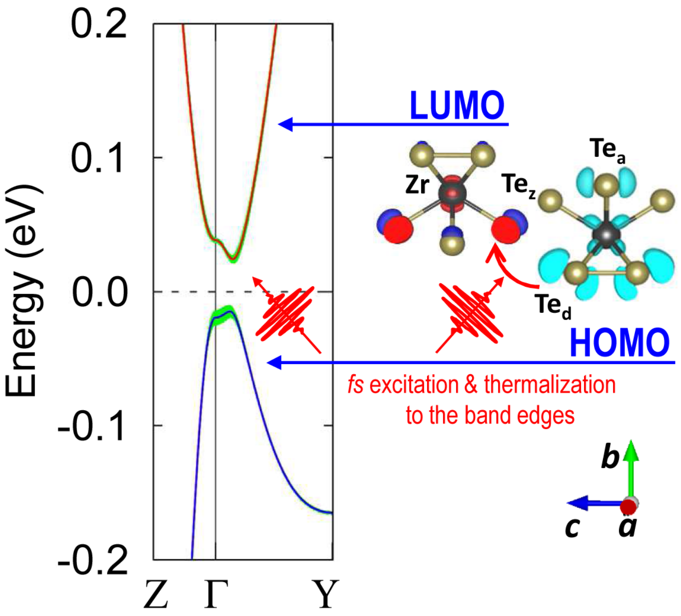

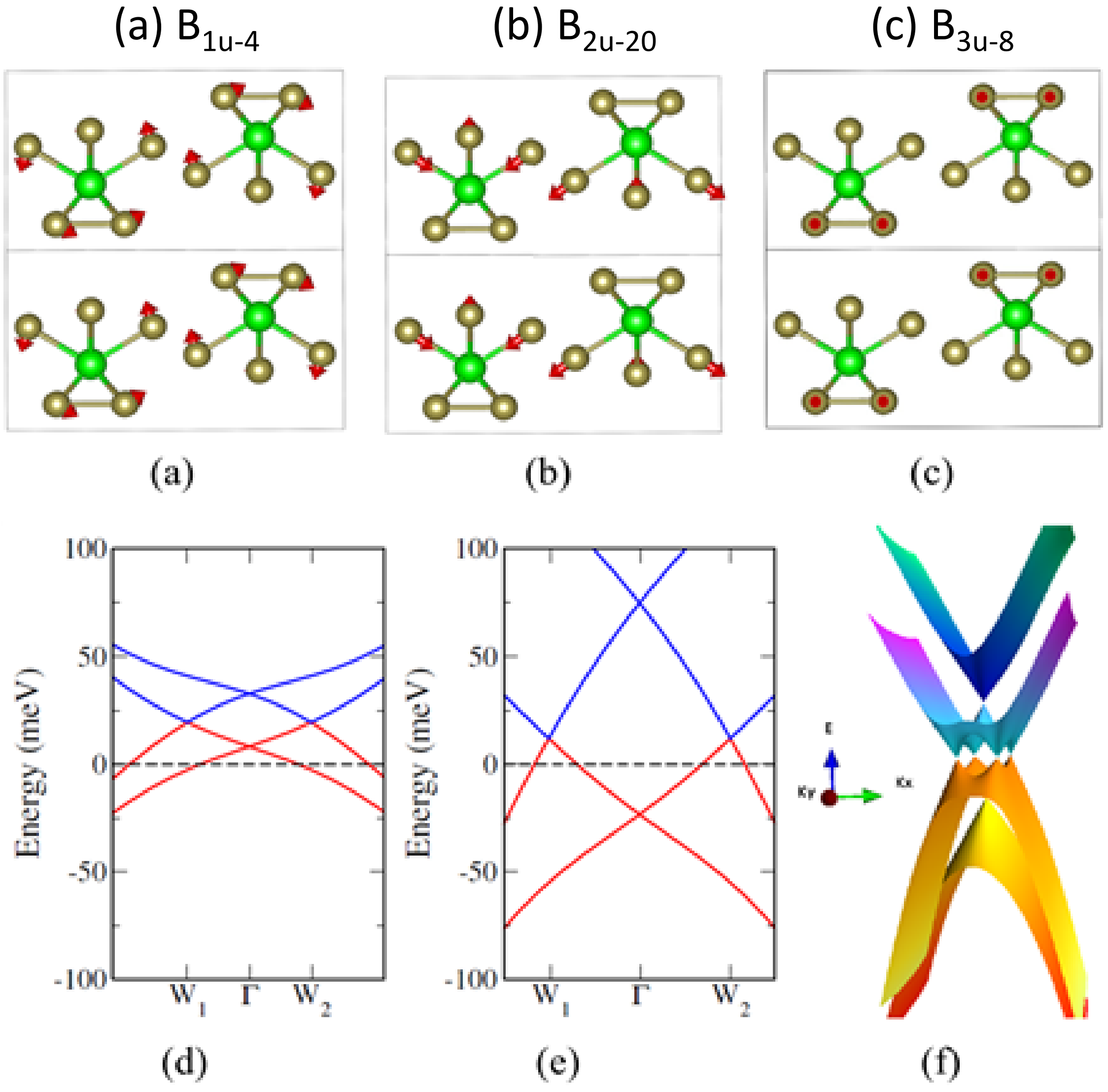

IR modes in $ZrTe_5$ projected on the b-c plane: (a) B_{1u-4} (b) B_{2u-20} and (c) B_{3u-8}; (d), (e) Band structure along W1-G-W2 direction for Q values of 1 and 4.5 respectively calculated from DFT for B_{1u-4} mode. (f), the bands forming the WPs are shown on the k_x - k_y.

Aryal, QL, et al, npj Computational Materials 8, 113 (2022).

Detection and manipulation of chirality in Weyl semimetal TaAs

TaAs

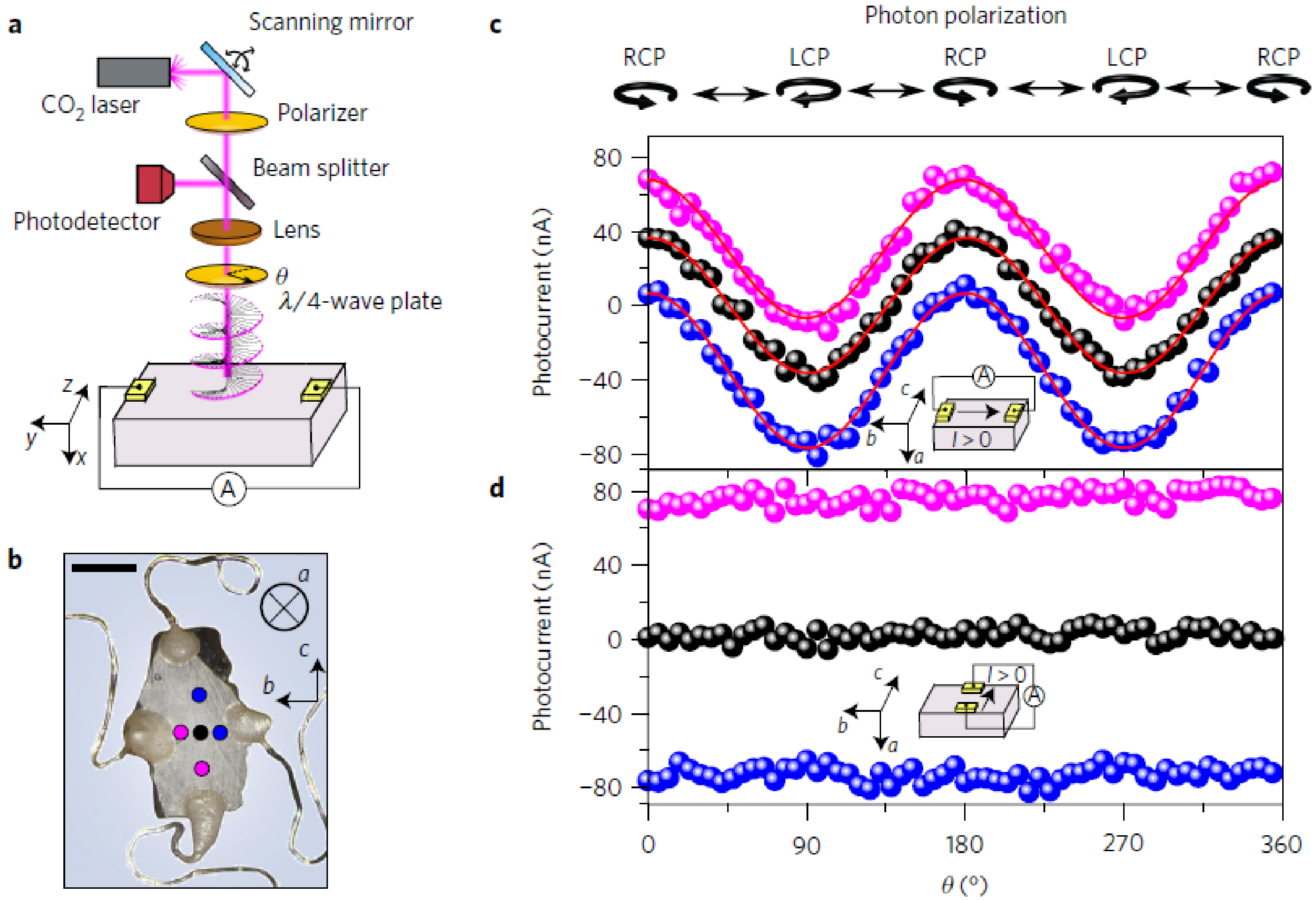

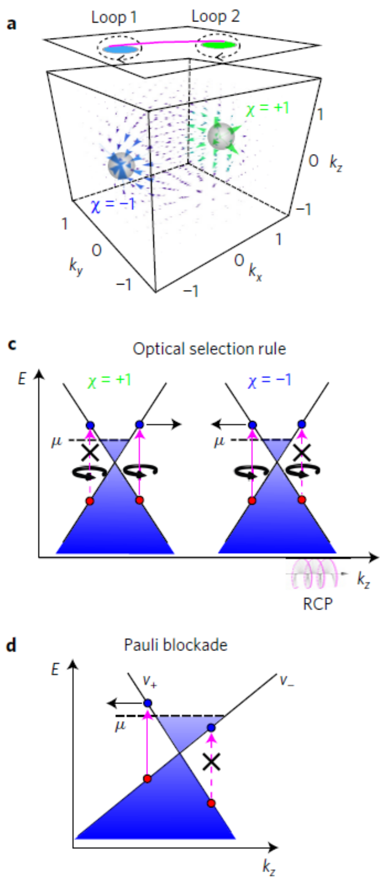

Ma, et al., Nature Physics **13**, 842 (2017)

A Light-induced Giant Dissipationless Topological Photocurrent in $ZrTe_5$

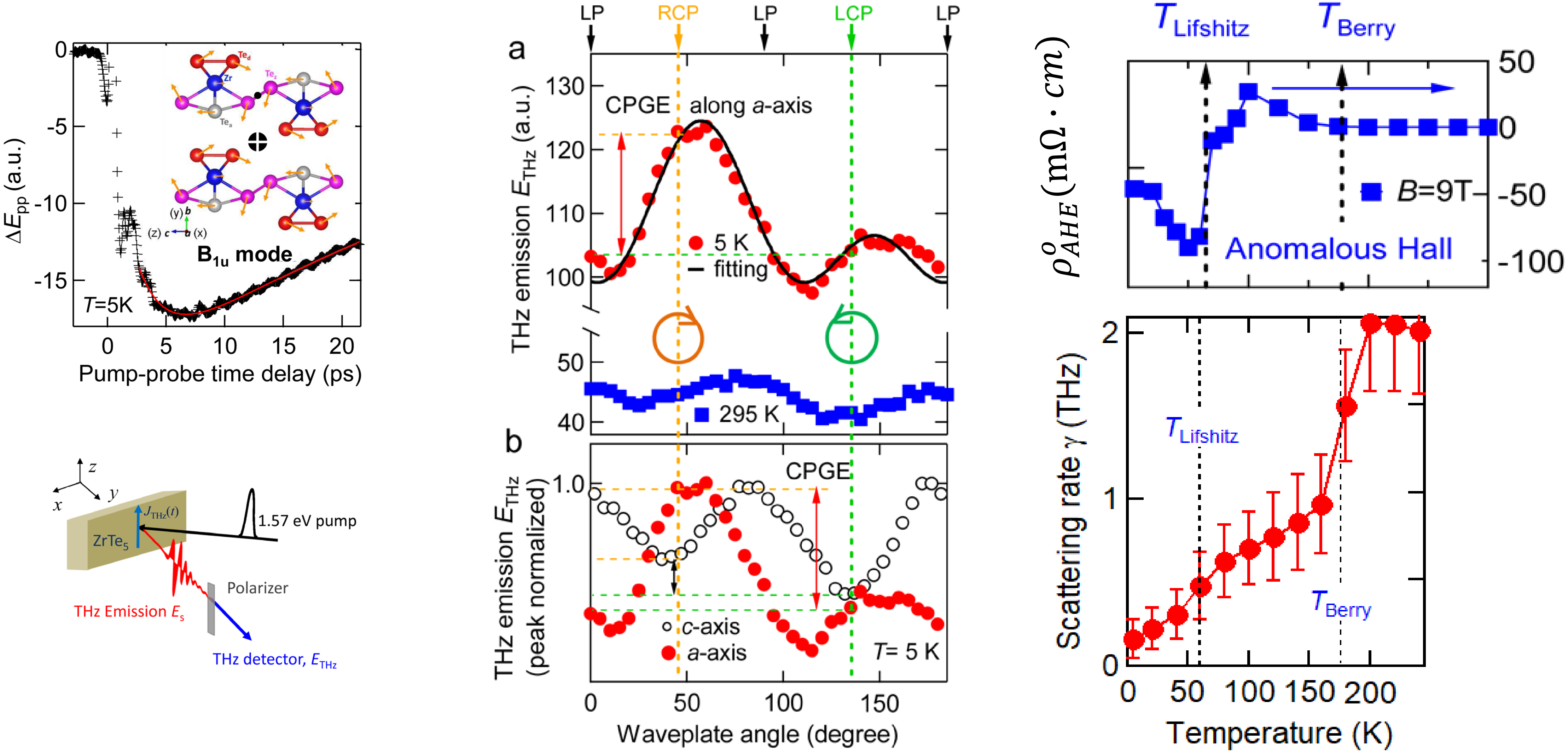

Luo, QL, et al. Nature Materials 20, 329 (2021)

Tunability of Weyl phases by phonons

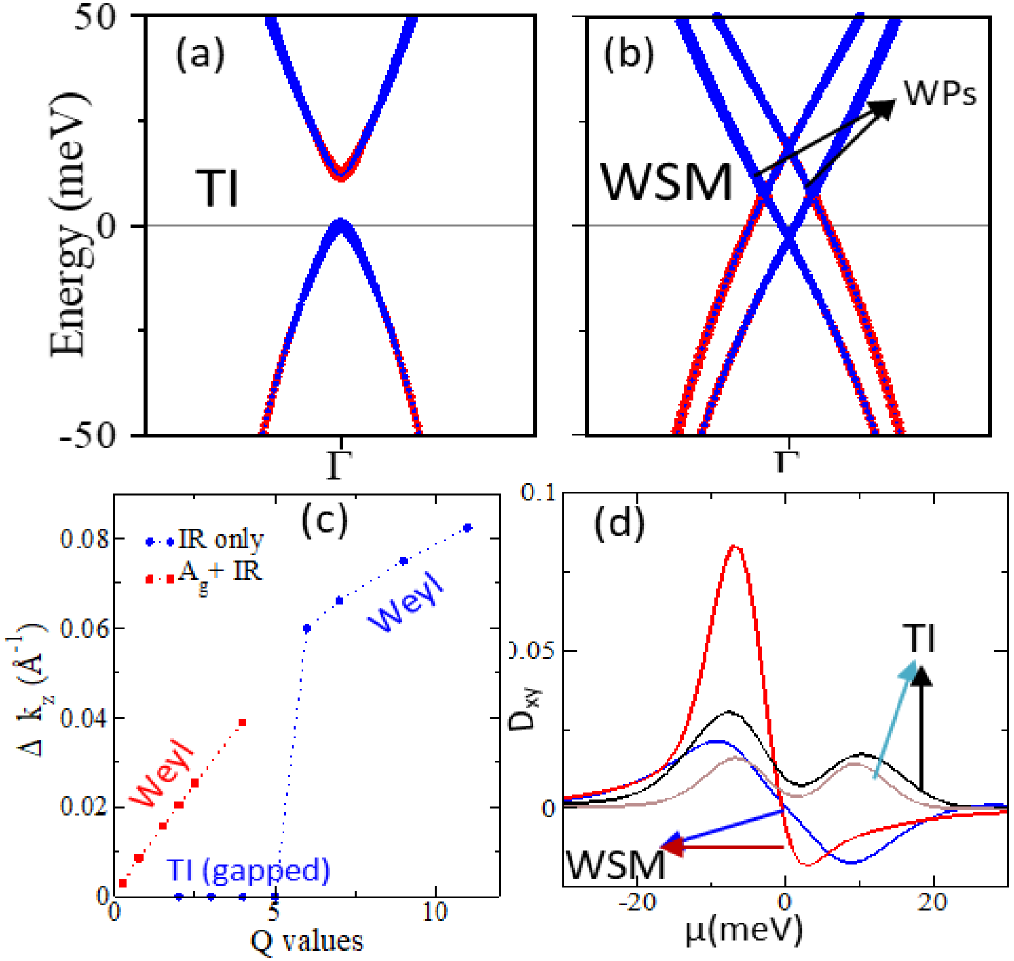

- The IR pumping threshold can be drastically reduced if used in conjunction with an A_g Raman-mode pumping that first drives the system towards the Dirac semimetal phase.

Figure (a, b) Evolution of the band structure of $ZrTe_5$ around Γ point with an IR mode lattice distortion *Q*=0 as a TI (**a**) and *Q*=1.5 showing Weyl points (WPs) (**b**). **(c)** Distance between the WPs when pumping from TI (blue) or DSM (red) phase. **(d)** Berry curvature dipole moment as a function of chemical potential for TI and WSM phases.

Aryal, QL, npj Computational Materials 8, 113 (2022).

Reaching Weyl phases faster by Raman + IR phonons

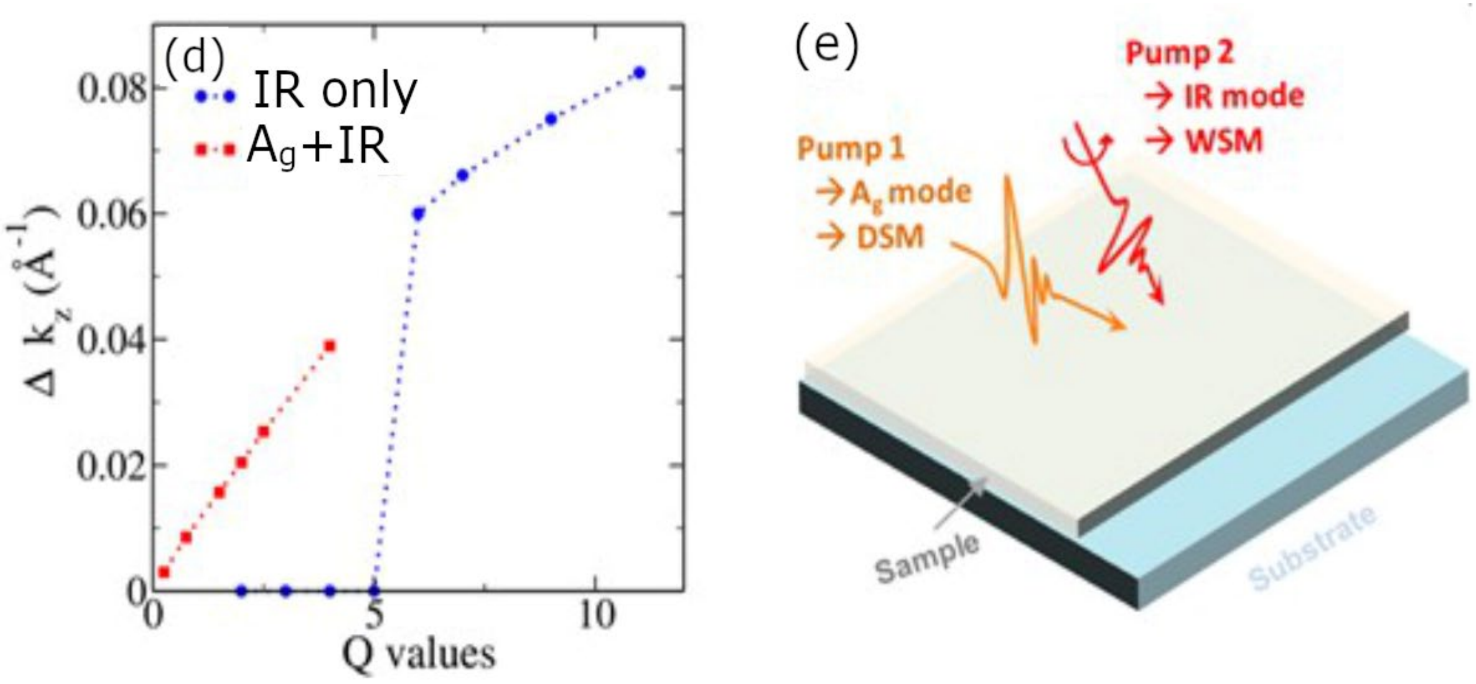

The IR pumping threshold can be drastically reduced if used in conjunction with an A_g Raman-mode pumping that first drives the system towards the Dirac semimetal phase.

Aryal, QL, npj Computational Materials 8, 113 (2022).

Chiral Qubit*

Chiral Qubit is a micron-scale ring made of a Weyl or Dirac semimetal, with the two base states describing chiral fermions circulating along the ring clockwise and counter-clockwise. A fractional magnetic flux through the ring induces a quantum superposition. The entanglement of qubits can be implemented through the circularly polarized THz frequency electromagnetic fields.

$$\hat{H} = \hbar\omega \left(-i\partial_\theta + \frac{\Phi}{\Phi_0} \right) \hat{\sigma}_z$$

$$|0\rangle = \frac{1}{\sqrt{2}} \left(|R\rangle + |L\rangle \right), |1\rangle = \frac{1}{\sqrt{2}} \left(|R\rangle - |L\rangle \right)$$

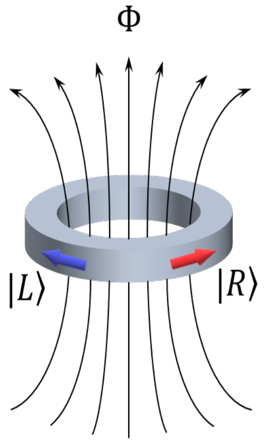

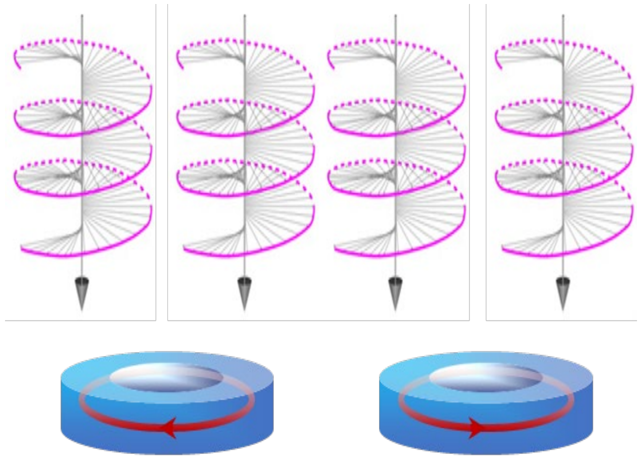

$$\alpha |L\rangle \quad + \quad \beta\, |R\rangle$$

*D. Kharzeev and QL “Quantum computing using chiral qubits” United States patent #10,657,456 B1 (2020);
D. Kharzeev and QL “The Chiral Qubit: quantum computing with chiral anomaly” arXiv:1903.07133

Superconducting qubit

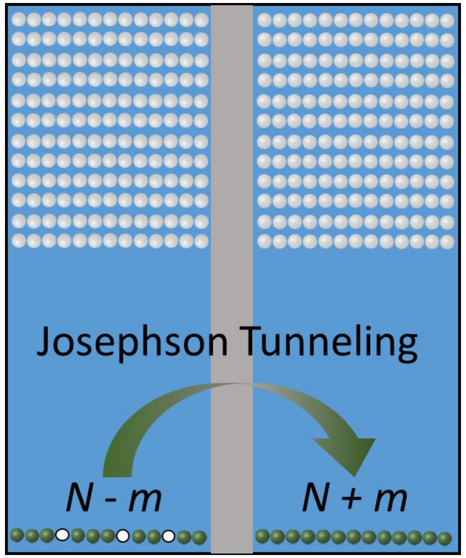

GHz energy gap
Microwave pulse

1 K ~ energy fluctuations 20 GHz

Chiral qubit

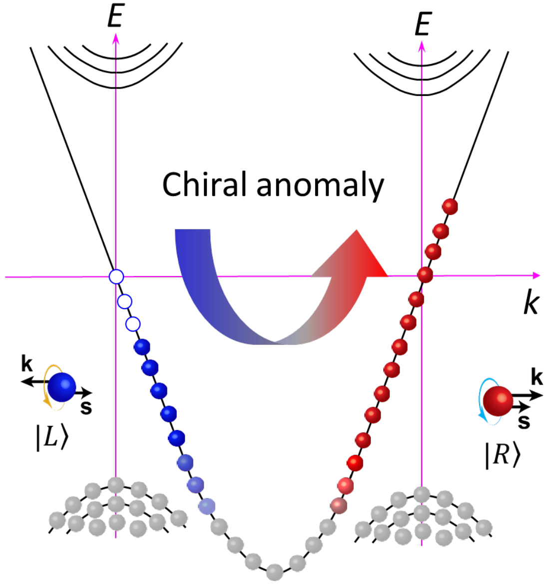

THz pulse

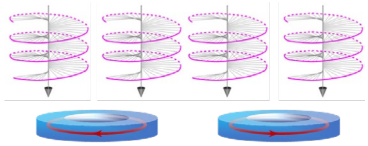

$\alpha|L\rangle + \beta\ |R\rangle$

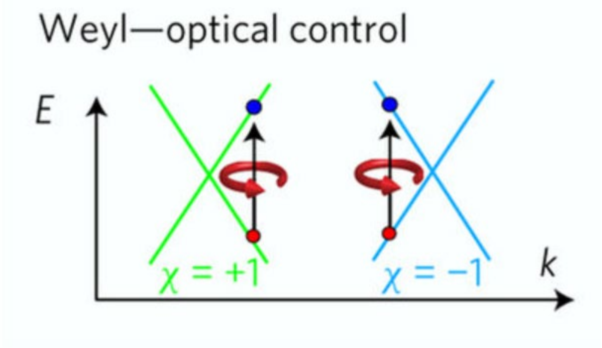

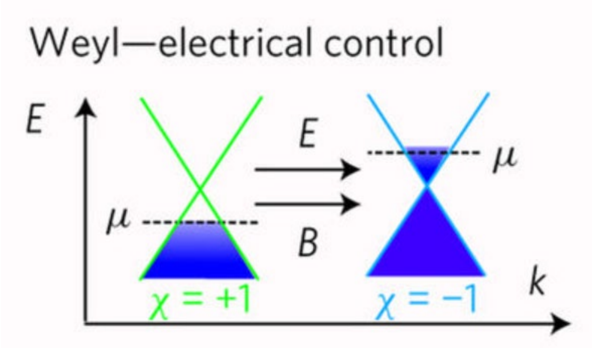

What do you need to build a quantum computer?

Di Vincenzo's Criteria*

Chiral qubit

Di Vincenzo's Criteria*	Chiral qubit
1. A scalable physical system with well-characterized qubits.	None
2. Qubit initialization.	~ OK, gate speed (THz) > 10,000 $\frac{1}{\tau}$
3. Long relevant decoherence times.	$\tau > 100\, ns$
4. A "universal" set of quantum gates.	Circular polarized light and duration
5. A qubit-specific measurement capability	Circular polarization of THz emission

DiVincenzo Fortschritte der Physik 48, 771 (2000)

Superconducting quantum circuit
Nonlinear circuit – Artificial Atom

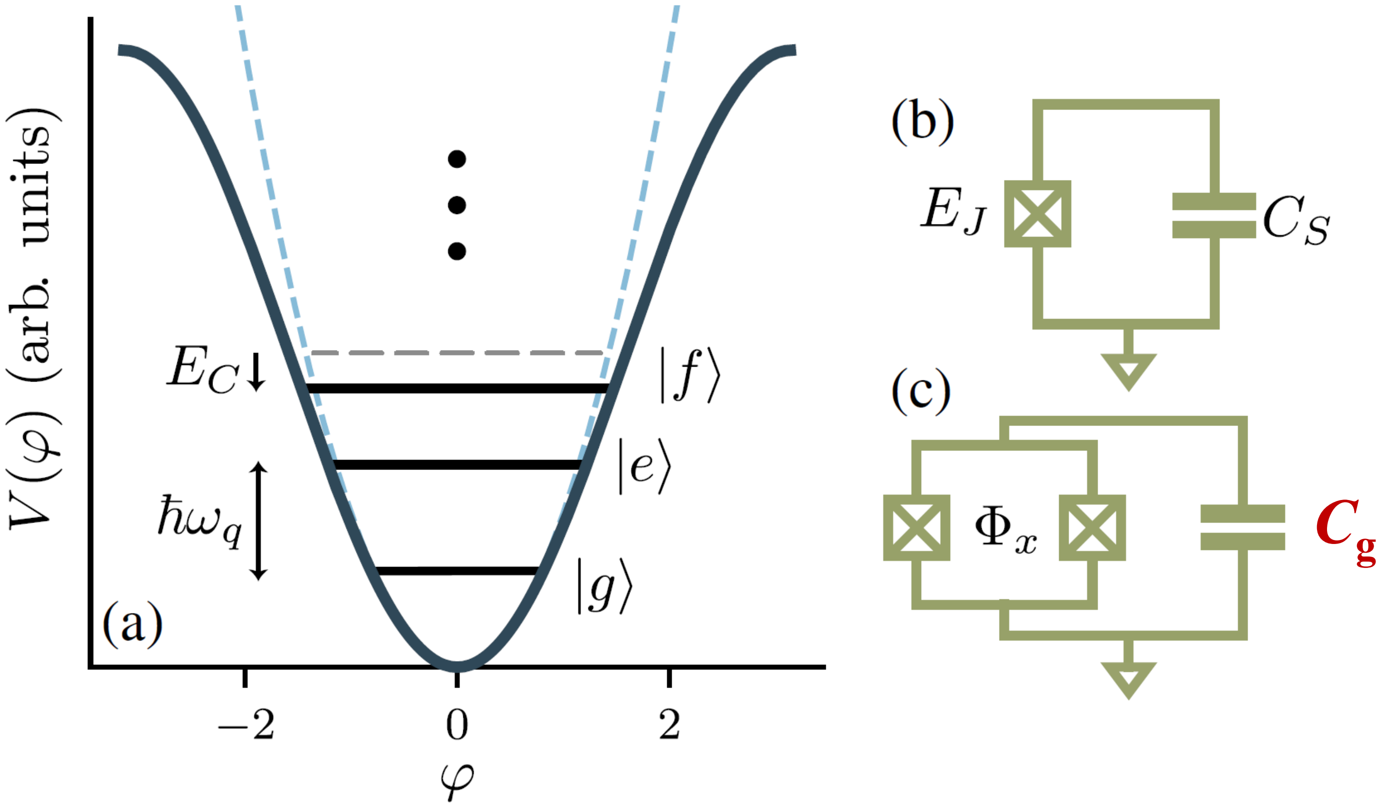

- If the nonlinearity and Q are large enough, we have an artificial atom
- If we restrict ourselves to $|g\rangle$ and $|e\rangle$, we have a qubit.
- By using a SQUID, the frequency of the transmon qubit becomes flux tunable.

Blais, Grimsmo, Girvin, and Wallraff: "Circuit quantum electrodynamics" Rev. Mod. Phys. **93**, 025005 (2021)

The spectrum of $\hat{H}_T$ is controlled by the ratio

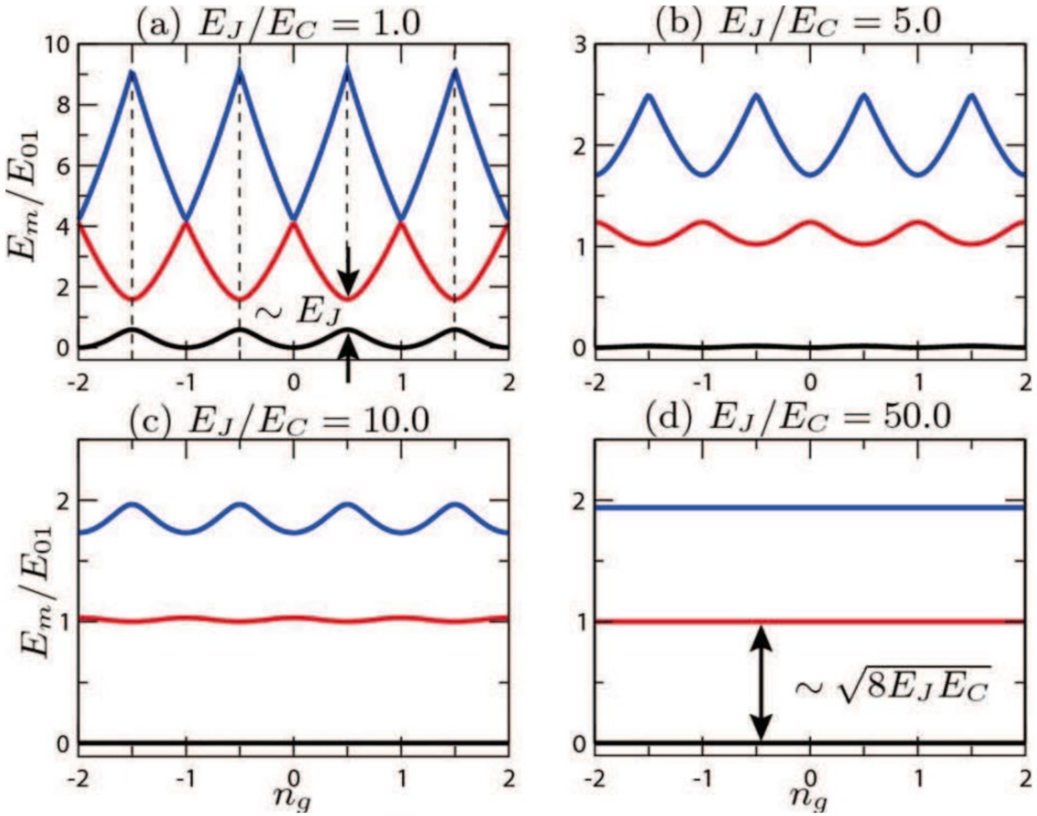

$$\hat{H}_T = \frac{\left(\hat{Q} - Q_g\right)^2}{2C_\Sigma} - E_J cos\left(2\pi\frac{\hat{\Phi}}{\Phi_0}\right)$$
$$= 4E_C\left(\hat{n} - n_g\right)^2 - E_J cos\left(2\pi\hat{\delta}\right)$$

Frequency difference $\omega_j - \omega_o\pi$ of the first three energy levels of the transmon Hamiltonian obtained from numerical diagonalization of the equation expressed in the charge basis $\left||n\rangle\right|$ for different $\frac{E_J}{E_C}$ ratios and a fixed plasma frequency $\frac{\omega_p}{2\pi} = 5\text{ GHz}$.

For large values of $\frac{E_J}{E_C}$ the energy levels become insensitive to the offset charge n_g.

$\frac{E_J}{E_C} \ll 1 \sim$ charge qubits, $\frac{E_J}{E_C} \gg 1 \sim$ transmon, (Typically $\frac{E_J}{E_C} \sim$ 20-80)

Blais, Grimsmo, Girvin, and Wallraff: “Circuit quantum electrodynamics” Rev. Mod. Phys. **93**, 025005

Tunable chiral qubits

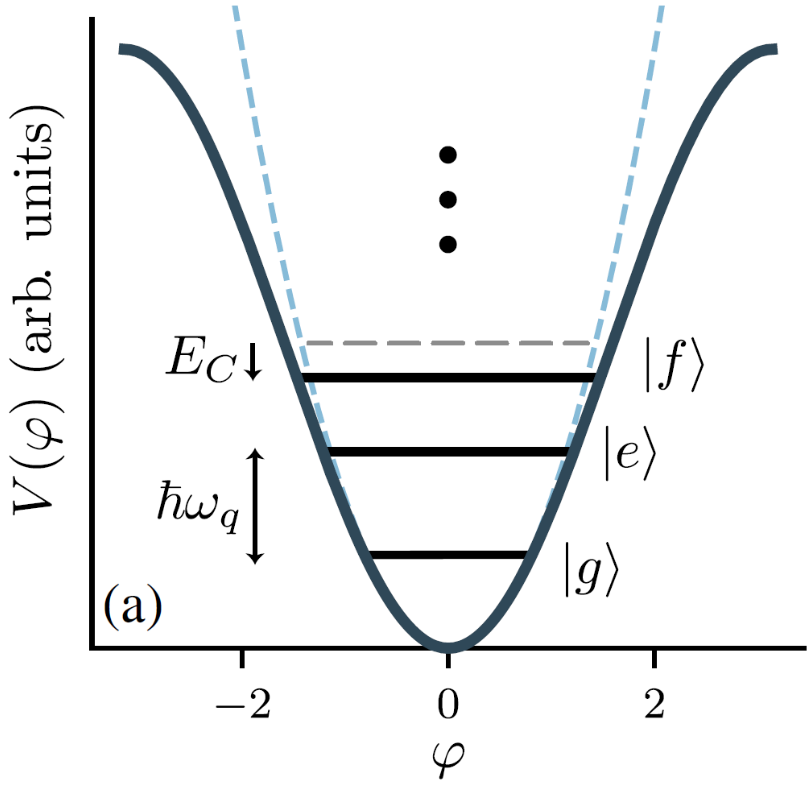

- Introduce nonlinearity, like a small mass term, m_g, ? => An artificial atom”
- Restricting ourselves to $|g\rangle$ and $|e\rangle$, we have a qubit.
- Gate m_g tuned controlled by strain, phonons, magnetic Weyl semimetal, magnetic impurity, etc

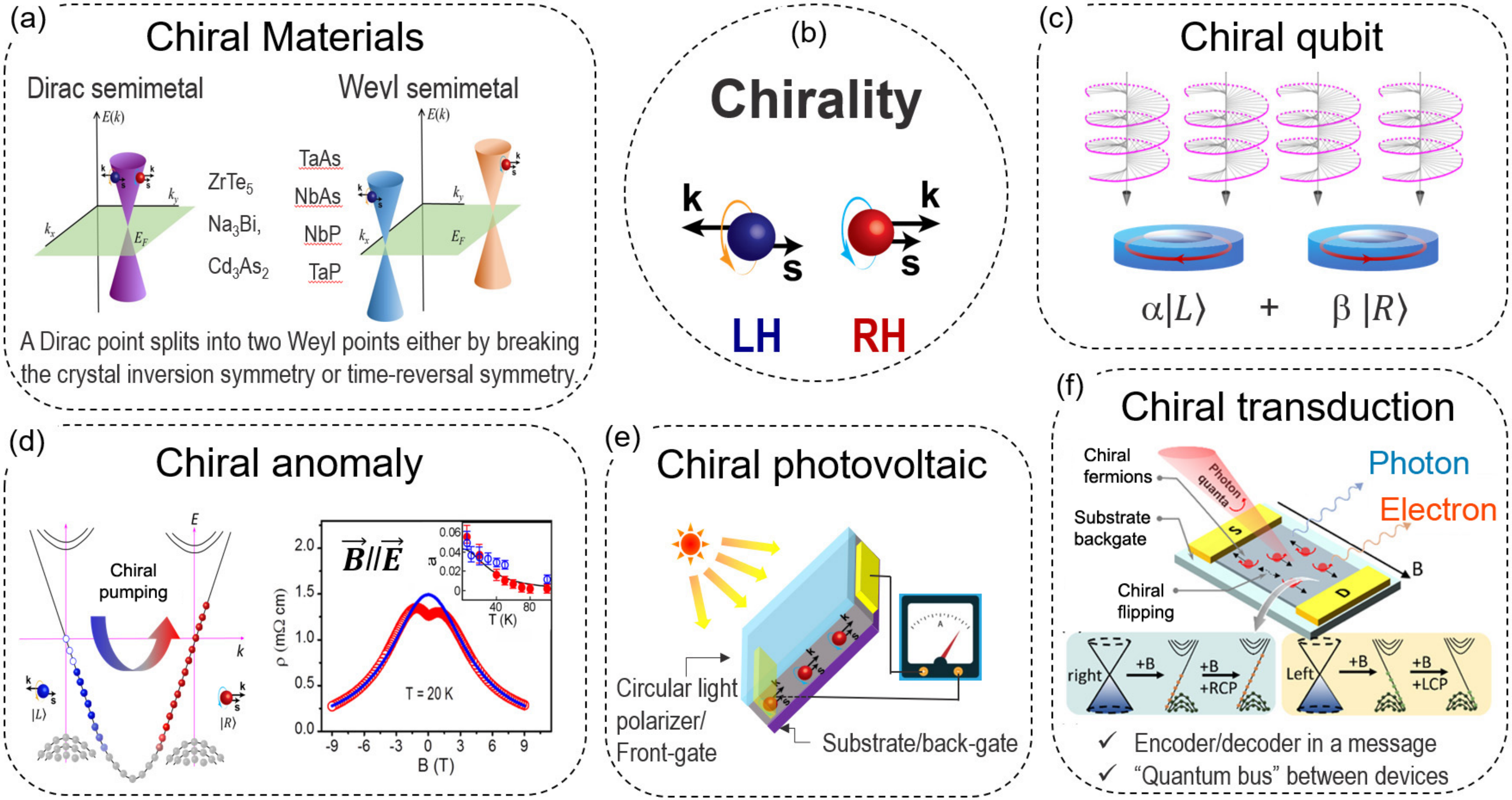

Q. Li “Dynamics of chiral fermions in condensed matter systems” A chapter in Chiral Matter: Proceedings of the Nobel Symposium 167, Pages 83-94, https://www.worldscientific.com/doi/10.1142/9789811265068_0007 published by World Scientific.

Concluding remarks

- Photoexcitation of phonon modes is shown to be an effective method to control topological states in $ZrTe_5$ This should be applicable to other topological systems
- Angular momentum coupling between circular polarized light and chiral fermions makes chirality effective quantum information carrier